JOURNAL OF SPACECRAFT AND ROCKETS
Vol. 44, No. 3, May–June 2007

Identification of Overpressure Sources at Launch Vehicle Liftoff Using an Inverse Method

B. Troclet*
EADS ST, 78133 Les Mureaux, France
and
S. Alestra,† I. Terrasse,‡ S. Jeanjean,† and V. Srithammavanh†
EADS CRC, 92150 Suresnes, France

DOI: 10.2514/1.21577

At liftoff, launch vehicles are subjected to a very severe overpressure and to an acoustic environment which can induce loads acting on payloads in the low-frequency domain (frequencies lower than 40 Hz). The overpressure starts at ignition of solid rocket motors. This overpressure phase is followed by the acoustic phase. The liftoff acoustic environment is generated by the rocket exhausts and by their impingement on the launch pad. For a numerical prediction of the acoustic environment, the European Aeronautic Defence and Space Company (EADS) has developed an inverse method via a time domain boundary integral equations approach using an optimal control method, with direct and adjoint equations. The corresponding discrete schemes are highly accurate and unconditionally stable. As an industrial application, the identification of sources of overpressure is shown, which occurs at solid rocket motor ignition ARIANE 5. Having localized and characterized the sources from overpressure phase measurements in the time domain, the complete pressure environment is recovered. By integrating the resulting pressures over all surfaces of the launchers, the loads created by the liftoff overpressure field can be estimated. To achieve this identification, the 511 ARIANE 5 flight, which was instrumented, has been chosen. After identification of the overpressure sources, the pressures restored by direct calculation are compared with measurements. Last, an analysis of the robustness of the approach is presented.

Nomenclature

A	=	source operator projection
A^i	=	operator projection A for Dirac source excited at time $= ti$
B	=	incident field operator projection
B^i	=	incident field operator B projection for Dirac source excited at time $= ti$
c	=	sound speed in the air
Do_k	=	delta of pressures computed for the kth couple of sensors
Do_{mes_k}	=	delta of pressures measured for the kth couple of sensors
e^i	=	Dirac source excited at time $= ti$ operator
H	=	Hessian approximation
it	=	iteration
$j(p) = J(O(p))$	=	cost function
$L(\,)$	=	Lagrangian
l	=	iteration optimizer
N	=	no. of solver time iterations
NDF	=	no. of degrees of freedom on the obstacle boundary
Ncoupl	=	no. of diametrically opposed pressure sensors
Nparam	=	no. of source parameters
N_{obs}	=	no. of pressure sensors
n	=	discrete current iteration
$O(p)(x,t)$	=	total pressure field computed
O_i	=	pressure at the ith receiver
$O_{\text{mes}}(x,t)$	=	measured observed pressure at sensors
$O^e_{\text{diff}}(x,t)$	=	scattered field outside the obstacle
$O^i_{\text{diff}}(x,t)$	=	scattered field inside the obstacle
$O^p_{\text{inc}}(x,t)$	=	incident field for source p
O^*	=	adjoint total field
O^*_i	=	adjoint field at the ith sensors
p	=	source parameter vector
p_i	=	component of excitation parameter at time $t = ti$
Q^*_k	=	scattered matrices adjoint posttreatment
R	=	integral surface operator
R^*_k	=	surface integral adjoint matrices
$S(p)$	=	boundary traces of the incident field source parameter p
t	=	time variable
U	=	acoustic pressure jump across the boundary
U^*	=	adjoint pressure jump
V^i	=	unitary jump pressure for Dirac source excited at time $= ti$
W^i	=	unitary pressure for Dirac source excited at time $= ti$
x, y	=	spatial variables in 3-D
x_0	=	location of source label $= p$
Γ	=	obstacle boundary
Δt	=	time step
Ψ	=	test function (in variational formulation)
Ω^e	=	exterior domain obstacle
Ω^i	=	interior domain obstacle
$\frac{\nabla j}{\nabla p_i}$	=	unitary gradient for Dirac source excited at time $= ti$

Received 6 December 2005; accepted for publication 26 May 2006. Copyright © 2006 by the American Institute of Aeronautics and Astronautics, Inc. All rights reserved. Copies of this paper may be made for personal or internal use, on condition that the copier pay the $10.00 per-copy fee to the Copyright Clearance Center, Inc., 222 Rosewood Drive, Danvers, MA 01923; include the code 0022-4650/07 $10.00 in correspondence with the CCC.

*Expert in Structural Analysis, Missile Structural Analysis Department.
†Research Development Engineer, Simulation Systems and Information Technology Department.
‡Manager of Applied Mathematics and High Performance Computing Team, Simulation Systems and Information Technology Department.

$\frac{\nabla j}{\nabla p}$ = gradient source parameter

I. Industrial Problem

DURING the liftoff phase, the launch vehicles, such as the ARIANE 5 launcher, are subjected to severe loads: the overpressure loads. The overpressure loads are among the most severe loads that a launcher can encounter during flight. The initial cause of these two load cases is the rocket exhaust and its interactions with the launch pad (see Figs. 1 and 2).

At rocket motor ignition, the sudden initiation of rocket exhausts in the launch ducts has a similar effect to the upward motion of a piston causing compressive waves which propagate outside the launch duct and, consequently, excite the launcher.

Regarding ARIANE 5, the overpressure at motor ignition is generated by the solid rocket boosters (SRB).

The overpressure is composed of the ignition overpressure (IOP), which emanates from the launch table, and of the duct overpressure (DOP), which emanates from the launch ducts. Figure 2 illustrates this point with a picture of the ARIANE 5 launch pad.

The overpressure is a deterministic load case, presenting discrete spikes at some particular frequencies depending on the geometrical configuration of the launch pad, with significant levels for frequencies lower than 20 Hz.

This low-frequency excitation excites the launch vehicle and induces quasi-static loads (QSL) at the payload/launcher interface (Fig. 3), which the payload has to endure. Consequently, it is important to predict these loads before launches (see [1–4]). The idea in this paper is to derive overpressure sources in the time domain directly from pressure measurements obtained during flights by an inverse method. The determination of overpressure sources by an inverse method is justified, because it is difficult to obtain accurate predictions by using Navier–Stokes codes due to the presence of waterfall at liftoff. Indeed, in the case of the ARIANE 5 given version, the propulsion system and the launch pad are identical from one flight to another one, but the upper part geometrical configurations, depending on the payload size, can be different.

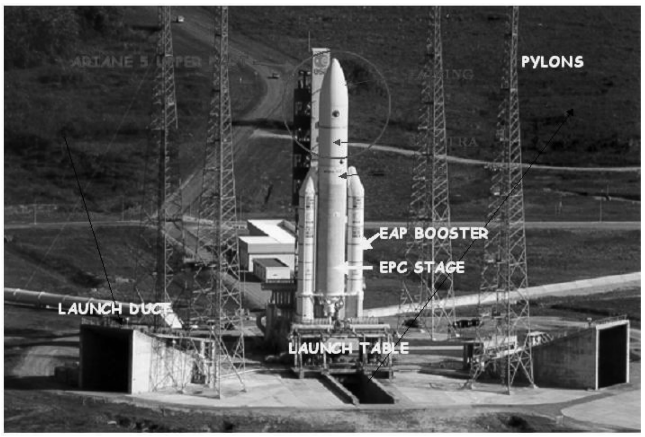

Fig. 1 ARIANE 5 and launch pad elements.

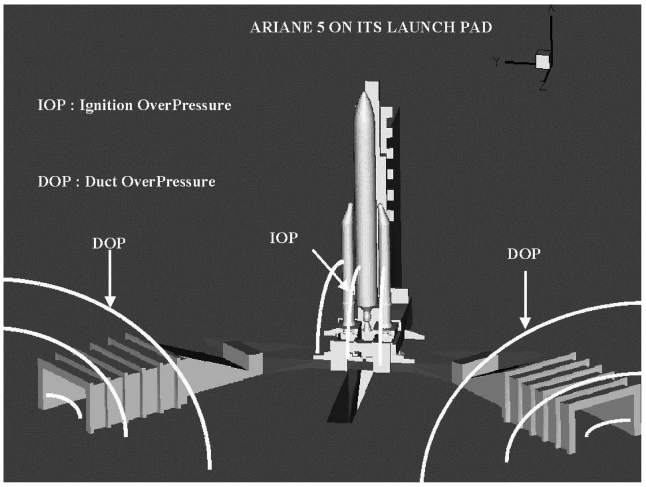

Fig. 2 Definition of the overpressure waves.

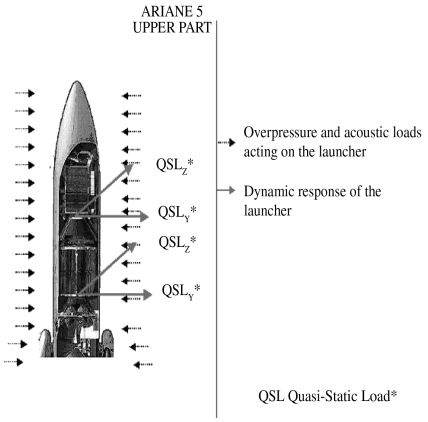

Fig. 3 Effects of the overpressure.

Having localized the sources from one ARIANE 5 flight measurements, it will be easy to rebuild the unsteady pressure field and to estimate the pressure levels at any point of the vehicle for other flights. By integrating the unsteady pressures over all surfaces of the launchers, the loads created by overpressure can be estimated. Consequently, the response of the launcher to this load case during the liftoff phase can be analyzed in the temporal domain by using any finite boundary elements software.

II. Inverse Source Problems with BEM (Boundary Element Method) in Time Domain

Inverse problems are found in many areas of engineering mechanics and there are many successful applications, for example, in geophysics, oil prospection, radar, electromagnetism, and specifically in acoustics, in sonar application, medical imaging, nondestructive testing, and characterization of material properties by ultrasonics.

Generally speaking, inverse problems are concerned with the determination of the input and the characteristics of a system, given certain aspects of its output. Mathematically, such problems are ill posed in that small changes in the data can produce large effects in the solution. Furthermore, even questions of whether a solution that corresponds to likely noisy data can exist and how many different solutions may exist that correspond to partial data sets need to be considered.

The enormous increase in computing power and the development of new computational schemes and powerful algorithms has made it possible to consider real-world problems of growing complexity and has led to a growing appetite to apply the techniques of inverse problems to ever more complicated physical problems.

We present now an inverse source method based on a powerful boundary element method in a time domain.

The development of numerical algorithms for time domain scattering problems, in which the incident fields are arbitrary functions of time, is important because generally, by studying the time domain problem directly (rather than taking the transform of frequency domain results) we can obtain a better understanding of scattering problems in general and also because a lot of information can be extracted with few (in the number of receivers) time domain measurements available.

The boundary element method is a technique which is widely studied in mathematics but which is strongly motivated by the demands of engineering analysis. The method is simple in concept: for many (classical) partial differential equations (PDEs), integral theorems can be used to represent the solution as a combination of boundary potentials, the unknown densities of which can be found by

solving numerically a system of (singular) integral equations which is posed only on the boundary of the domain. The method is extremely attractive for problems on infinite regions such as often arise in (electromagnetic or acoustic) scattering problems.

The problem of concern is the identification of acoustic sources in the time domain from in-flight measurements. As we define a priori locations of the sources from past experience, the objective of the computations by using the inverse method is to determine the evolution versus time of the pressure amplitudes of sources. In a previous paper [4], the methodology has been validated on the 503 ARIANE 5 flight, in low-frequency acoustics for the ARIANE 5 acoustic source identification on the data from the 503 ARIANE 5 flight: previous results were very promising and have showed a satisfactory identification of the sources in the 0–40 Hz frequency domain (source function at each time step), with partial acoustic data (launcher upper part sensors).

In this paper, the new developments of this inverse computation method have the following objectives:

1) Through an optimization loop, to identify overpressure sources, which restore the measured pressures and above all, the difference of pressure between diametrically opposite points therefore (to complete the identification of sources by optimizing on p and Δp). Indeed, it is the difference of pressure between diametrically opposite points, which dynamically excite the launcher.

2) To complete the validation of the inverse method with regards to the overpressure by performing a robustness analysis.

3) To reduce the computation times by decomposing the sources parameters vector into a base of unitary sources (multilinear process). Global time computation can be reduced by a factor of 10.

Let us consider that the time domain content of the source, at point x_0, is represented by a real function $p(t)$, which is sampled over time $p = (p_1; \ldots, p_p, \ldots, p_{N\text{param}})$, where the subscripts refer to the sampled time Nparam, the number of unknown parameters regarding the pressure amplitudes of sources. Nparam is often equal to N, the sample size used for solving the direct problem. These sampled values will be the control parameter variables for the optimization process.

Our theory is formulated for one source, for simplification, but we can easily generalize to many sources. Let $p(t)$ be the source parameter

$$p(t) = \begin{pmatrix} p_1 = p(\Delta t) \\ \vdots \\ p_{N\text{param}} = p(N\Delta t) \end{pmatrix} \tag{1}$$

and $O_{\text{inc}}(p)$ the corresponding incident pressure field:

$$O_{\text{inc}}(p)(x,t) = \frac{p(t - |x - x_0|/c)}{4\pi|x - x_0|} \tag{2}$$

The scattering effect of transient acoustic waves in a fluid medium by a submerged rigid object is taken into account. Let Ω^i be a three-dimensional object with a regular (without tip) bounded surface $\Gamma = \partial\Omega^i$.

Let $\Omega^e = R^3 Omega^i$ denote the exterior domain occupied by the fluid medium. We denote by O^e_{diff} the scattered acoustic pressure of the incident field $O_{\text{inc}}(p)$.

Therefore, we have the following initial boundary value problem:

$$\begin{cases} \frac{1}{c^2}\frac{\partial O^e_{\text{diff}}(x,t)}{\partial t^2} - \Delta O^e_{\text{diff}}(x,t) = 0 & \text{in } \Omega^e \times R^+ \\ O^e_{\text{diff}}(x,0) = \frac{\partial O^e_{\text{diff}}}{\partial t}(x,0) = 0 & \text{in } \Omega^e \\ \frac{\partial O^e_{\text{diff}}}{\partial n} = -\frac{\partial O_{\text{inc}}}{\partial n}(p)(x,t) & \text{on } \Gamma \times R^+ \end{cases} \tag{3}$$

where n denotes the unit normal vector to Γ, oriented from domain Ω^I to Ω^e, and c is the speed of sound in the medium. There are many methods to solve this problem, using boundary integral equations. Many authors have developed these methods in acoustics [5–7].

Some authors [8] have implemented the variational approximation of time domain integral equations (TDIE) in acoustics and some others (see [9,10]) have worked on the hybridization of TDIE with local PDEs.

Each method consists of looking for the solution as a prescribed combination of surface-retarded potentials and expressing the boundary condition as a function of the densities of the potentials. Equivalently, this corresponds to associating to the exterior problem an appropriate interior problem.

We associate the *exterior* problem with an appropriate *interior* problem with O^i_{diff} in Ω^I.

$$\begin{cases} \frac{1}{c^2}\frac{\partial O^i_{\text{diff}}(x,t)}{\partial t^2} - \Delta O^i_{\text{diff}}(x,t) = 0 & \text{in } \Omega^i \times R^+ \\ O^i_{\text{diff}}(x,0) = \frac{\partial O^i_{\text{diff}}}{\partial t}(x,0) = 0 & \text{in } \Omega^i \\ \frac{\partial O^i_{\text{diff}}}{\partial n} = -\frac{\partial O^p_{\text{inc}}}{\partial n} & \text{on } \Gamma \times R^+ \end{cases} \tag{4}$$

It is well known that the scattered field O^e_{diff} has the following representation formulation, using the near-field scattered operator Q:

$$O^e_{\text{diff}}(x,t) = QU = -\frac{1}{4\pi}\int_\Gamma n_y \cdot \nabla_x \frac{U(y, t - |x-y|/c)}{|x-y|}\,\mathrm{d}y \quad \forall\ x \in \Omega^i \cup \Omega^e \tag{5}$$

where $U = O^i_{\text{diff}} - O^e_{\text{diff}}$ is the jump O^e_{diff} crossing Γ, and $\tau = t - |x - y|$ is the *retarded time*. Using a *formula* to compute the traces of O^e_{diff} $\Gamma \times R^+$, as a function of U, and introducing the boundary conditions, one obtains the *boundary integral equation* for the unknown function U:

$$RU(x,t) = S(p)(x,t) \quad \forall\ (x,t)\Gamma \tag{6}$$

with the surface operator R, a double layer integral operator, and S the projection (traces) of incident field on the surface boundary Γ.

$$S(p)(x,t) = \int_\Gamma \frac{\partial O^p_{\text{inc}}(x,t)}{\partial n}\,\mathrm{d}y \tag{7}$$

We have for R:

$$RU(x,t) = -\lim_{x' \in \Omega^+ \to x} n_x \cdot \nabla_{x'} \frac{1}{4\pi}\int_\Gamma n_y \cdot \nabla_{x'}\left(\frac{U(y, t - |x'-y|/c)}{|x'-y|}\right)\mathrm{d}\sigma_y \tag{8}$$

It should be noted that the operator R contains a *hypersingular kernel* and has to be defined properly. One can do this by using a method of regularization.

An equivalent formulation of Eq. (6) is developed in [11–16], and can be written, with function U in $H^2(R+, H^{1/2}(\Gamma))$, such that, for all Ψ in the same space:

$$\begin{aligned} &\int_{\Re}\int_{\Gamma\times\Gamma} \frac{\boldsymbol{n}(x)\boldsymbol{n}(y)}{4\pi|x-y|}\frac{\partial^2 U}{\partial t^2}\left(y, t - \frac{|x-y|}{c}\right)\frac{\partial \Psi}{\partial t}(x,t)\,\mathrm{d}x\,\mathrm{d}y\,\mathrm{d}t \\ &\quad + c^2\int_{\Re}\int_{\Gamma\times\Gamma} \frac{\mathrm{curl}_\Gamma U}{4\pi|x-y|}\left(y, t - \frac{|x-y|}{c}\right)\mathrm{curl}_\Gamma \frac{\partial \Psi}{\partial t}(x,t)\,\mathrm{d}x\,\mathrm{d}y\,\mathrm{d}t \\ &\quad = \int_{\Re}\int_\Gamma \left(\sum_{p=1}^{\text{NS}} \frac{\partial O^p_{\text{inc}}(x,t)}{\partial n}\right)\frac{\partial \Psi}{\partial t}(x,t)\,\mathrm{d}x\,\mathrm{d}t \end{aligned} \tag{9}$$

Equation (9) is solved in space by a surface finite element method. The boundary Γ of the object is meshed with N_h triangular elements. A $P1$ discretization in space surface finite element method and time is used. Each spatial basis function is associated with one vertex.

The boundary Γ of the object is meshed by using triangular elements.

Important remark: now, we use for the discrete value of functions U, $S_{\text{inc}}, S(p), O(p), O_{\text{inc}}(p)$ the following abusive notations:

$U(it) = U(it * \Delta t)$ for the U acoustic pressure jump at real time $it * \Delta t$ and corresponding numerical scheme iteration number it, as an example, considering that the total time T is discretized by N time steps Δt.

Therefore $T = N * \Delta t$, and the values of the previous acoustic quantities are taken at discrete time $it * \Delta t$, and referenced in the numerical schemes, by the integer it time index, as a simplified notation. The method is described in some detail in [11,16], and its implementation has confirmed stability in a wide range of situations and for large run times never reached before.

Therefore a direct scheme is unconditionally stable.

Finally, the discretized direct problem (9) consists of two main steps as follows:

1) Computation of the pressure jump U by the discretized integral equation (6) operators Rk, and of the excitation S, for all integers it from 1 to NT, by the following time marching matrix system, solved at each time step, by inversion of the matrix R_0:

$$R_0 U(it) = \sum_{k=1}^{it} R_k U(it-k) + S(p)(it) \tag{10}$$

Moreover, all the acoustic matrices are real, sparse, and symmetric.

2) Computation of the radiating posttreatment equation (5) and computation of the acoustic pressure O by using the discretized scattered operator Qk and accounting for the O_{inc} incident field contribution, for all it from 1 to NT:

$$O(p)(it) = \sum_{k=1}^{it} Q_k U(it-k) + O_{\text{inc}}(p)(it) \tag{11}$$

The quadratic error or cost function $j(p)$, depending on the source parameters p, is defined by

$$J(O(p)) = j(p) = \min_{q=X} j(q) = \tfrac{1}{2}\|O(q) - O_{\text{mes}}\|^2 \tag{12}$$

with

$$\begin{aligned} J(O(q)) &= \frac{1}{2}\langle O(q) - O_{\text{mes}}, O(q) - O_{\text{mes}}\rangle_{1*1} \\ &= \frac{1}{2}([{}^t(O(q) - O_{\text{mes}})]_{1*N\text{obs}}[O(q) - O_{\text{mes}}]_{N\text{obs}*1}) \\ &= \frac{1}{2}\sum_{it=0}^{NT}([{}^t(O(q) - O_{\text{mes}})](it)_{1*N\text{obs}}[O(q) - O_{\text{mes}}](it)_{N\text{obs}*1}) \end{aligned} \tag{13}$$

By introducing the adjoint variables U^*, O^* or the Lagrange multiplier, the classical Lagrangian formulation is obtained (see [12,17,18])

$$\begin{aligned} &L(p, U, O, U^*, O^*) \\ &= J(O) + \left\langle U^*(it), \left(R_0 U(it) - \sum_{k=0}^{it} R_k U(it-k) - S(p)(it)\right)\right\rangle_1 \\ &+ \left\langle O^*(it), \left(O(p)(it) - \sum_{k=0}^{it} Q_k U(it-k) - O_{\text{inc}}(p)(it)\right)\right\rangle_2 \end{aligned} \tag{14}$$

with the two following discrete scalar products for all degrees of freedom ($1 \cdots \text{NDF}$) and all sensors ($1 \cdots N\text{obs}$):

$$\langle a, b\rangle_1 = \sum_{t=0}^{NT} [{}^t(a^*)]_{1*\text{NDF}}(it)[b]_{\text{NDF}*1}(it) \tag{15}$$

$$\langle c, d\rangle_2 = [{}^t c]_{1*N\text{obs}}[d]_{N\text{obs}*1} = \sum_{it=0}^{NT} [{}^t c](it)_{1*N\text{obs}}[c](it)_{N\text{obs}*1} \tag{16}$$

We know that if (p, U, O, U^*, O^*) is a saddle point of the Lagrangian, p is at least a local minimum of the constrained cost function. With the optimality conditions written for U^* and O^*, we obtain the discrete adjoint equations:

$$\begin{cases} O^*(it) = -\frac{\text{d}J(O)}{\text{d}O} = -(O(p) - O_{\text{mes}})(it) \\ (R_0)^* U^*(it) = \sum_{k=0}^{N-it} (R_k)^* U^*(it+k) + \sum_{k=0}^{N-i} (Q_k)^* U(it+k) O^*(p)(it+k) \end{cases} \tag{17}$$

Except for the time evolution system direct (forward) and adjoint (backward), codes have exactly the same properties. Therefore, the adjoint scheme is also unconditionally stable.

Under the constrained direct equations, the Lagrangian (14) reduces to cost function:

$$j(p) = J(O(p)) = L(p, U(p), O(p), U^*(p), O^*(p)) \tag{18}$$

and so it becomes

$$\frac{\nabla j}{\nabla p} = \frac{\nabla J(O(p))}{\nabla p} = \frac{\partial L(p, U(p), O(p), U^*(p), O^*(p))}{\partial p} \tag{19}$$

But we have (direct and adjoint systems)

$$\frac{\partial \text{L}}{\partial U} = \frac{\partial \text{L}}{\partial O} = \frac{\partial \text{L}}{\partial U^*} = \frac{\partial \text{L}}{\partial O^*} = 0 \tag{20}$$

and by derivation of L, we obtain

$$\frac{\nabla j}{\nabla p} = -\left\langle U^*, \frac{\partial S(p)}{\partial p}\right\rangle - \left\langle O^*, \frac{\partial O_{\text{inc}}(p)}{\partial p}\right\rangle \tag{21}$$

By using the linear operator:

$$S(p) = Ap \qquad O_{\text{inc}}(p) = Bp \tag{22}$$

the gradient formulas become

$$\begin{aligned} \left[\frac{\nabla j}{\nabla p}\right](it)_{1*N\text{param}} &= -\langle U^*, A\rangle_{1*N\text{param}} - \langle O^*, B\rangle_{1*N\text{param}} \\ &= -[{}^t U^*]_{1*\text{NDL}}[A]_{\text{NDF}*N\text{param}}(it) - [{}^t O^*]_{1*N\text{obs}}[B]_{N\text{obs}*N\text{param}}(it) \end{aligned} \tag{23}$$

The expression of the gradients is now completely established. Starting with an initial guess for the estimated parameter p_0, a quasi-Newton optimizer is used to update the parameter value p

$$(p)^{l+1} = (p)^l - \left[H^{-1}\left(\frac{\nabla j}{\nabla p}\right)\right]^l \tag{24}$$

with H^{-1} a positive definite matrix, approximating the inverse of the Hessian of the cost function, and the gradient value is computed by formula (21), for the optimizer step l.

The goal is to find the optimal p_{opt}. A global view of the minimization process is shown Fig. 4.

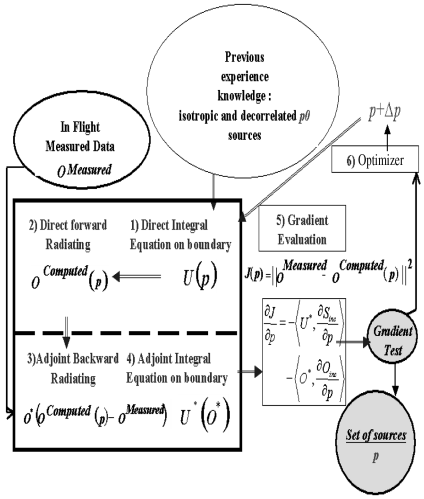

Fig. 4 Global scheme of the inverse process minimization loop.

We can reduce the computation times by decomposing the source parameters vector into a base of unitary sources (multilinear process) $p = \sum_i p_i e^i$ with e^i an element of the canonical basis. e^i is an elementary Dirac excitation at time $= ti$.

Then, using the linearity of the operators source $S(p)$ and incident field $O_{\mathrm{inc}(p)}$, we have

$$\begin{aligned} S(p) &= Ap = \sum_{i=1}^{n} p_i (Ae^i) = \sum_{i=1}^{n} p_i A^i \\ O_{\mathrm{inc}}(p) &= Bp = \sum_{i=1}^{n} p_i (Be^i) = \sum_{i=1}^{n} p_i B^i \end{aligned} \tag{25}$$

with

$$A^i = Ae^i \qquad B^i = Be^i \tag{26}$$

The unitary jump pressures V^i are solutions of the BEM integral equation:

$$R_0 V^i(it) = \sum_{k=1}^{it} R_k V^i(it-k) + A^i(it) \tag{27}$$

and then the unitary pressure solutions W^i are

$$W^i(it) = \sum_{k=1}^{it} Q_k V^i(it-k) + B^i(it) \tag{28}$$

and the total pressure $O(p)$ can be computed with the unitary pressure solutions W^i

$$O(p)(it) = \sum_i p_i W^i(it) \tag{29}$$

All the W^i functions can be deduced by the W^0 unitary solutions computed by the Dirac excitation at time $t = 0$, n by a time translation.

Also the gradients have a multilinear expression

$$\frac{\nabla j}{\nabla e^i} = -\sum_{it} \langle -(O(p) - O_{\mathrm{mes}})(it), W^0(it-i) \rangle e^i \tag{30}$$

and the global gradient vector can be recomposed for all components parameters, with these unitary gradients.

These unitary solutions W^i and particularly W^0 are computed before the optimization loop. During the optimization process, for an updated parameter p, these unitary solutions are used to compute the BEM pressure solution $O(p)$ for this parameter p, without having to compute a BEM system. Consequently, the computation global time is then reduced by a factor of 10 in the cases of interest.

We have completed the identification of sources by optimizing on p (pressures) and $DO(p)$ (differences of pressures between opposite points; indeed, in the low-frequency domain, the launch vehicle is excited by the differences of pressure between opposite points). Let us consider Ncoupl couples of opposite sensor points. K is taking values from 1 to Ncoupl, so that

1) $k = 1$ stands for sensors $i1$, $j1$;
2) $k = 2$ stands for sensors $i2$, $j2$;
3) $k = N$coupl stands for sensors iNcoupl, jNcoupl.

Then we set

$$\begin{aligned} Do_1 &= O_{i1} - O_{j1} \qquad Do_{\mathrm{mes}} i_1 = O_{\mathrm{mes}i1} - O_{\mathrm{mes}j1} \\ Do_2 &= O_{i2} - O_{j2} \qquad Do_{\mathrm{mes}2} = O_{\mathrm{mes}i2} - O_{\mathrm{mes}j2} \\ Do_{N\mathrm{coupl}} &= O_{iN\mathrm{coupl}} - O_{jN\mathrm{coupl}} \\ Do_{\mathrm{mes}N\mathrm{coupl}} &= O_{\mathrm{mes}iN\mathrm{coupl}} - O_{\mathrm{mes}jN\mathrm{coupl}} \end{aligned} \tag{31}$$

The cost function $j(p)$ Eq. (12) is then augmented by the differences of pressure terms:

$$\begin{aligned} J(O(p)) &= j(p) \\ &= \frac{1}{2}\|O(p) - O_{\mathrm{mes}}\|^2 + \frac{1}{2}\sum_{k=1}^{N\mathrm{coupl}} \|Do_k(p) - Do_{\mathrm{mes}k}\|^2 \end{aligned} \tag{32}$$

Consider that the kth couple of sensors are defined by the sensors i and j, and then we have $k(1) = i$, $k(2) = j$ and

$$Do_k = O_{i1} - O_{j1} \tag{33}$$

After derivation of the cost function $j(p)$, the adjoint field pressure O^* is updated for sensor i and sensor j, due to the delta of the pressure term. The backward adjoint continuous equation becomes

$$\begin{aligned} O_i^* &= -(O_i(p) - O_{\mathrm{mes}i}) - \sum_{k=1,k(1)=i}^{N\mathrm{couple}} (Do_k(p) - Do_{\mathrm{mes}k}) \\ O_j^* &= -(O_j(p) - O_{\mathrm{mes}}) + \sum_{k=1,k(2)=j}^{N\mathrm{coupl}} (Do_k(p) - Do_{\mathrm{mes}k}) \end{aligned} \tag{34}$$

The complete discrete expression of the adjoint system is, at the iteration scheme number it,

$$\begin{cases} O_i^*(it) = -(O_i(p) - O_{\mathrm{mes}i})(it) - \sum_{k=1,k(1)=i}^{\mathrm{Ncoupl}} (Do_k(p) - Do_{\mathrm{mes}k})(it) \\ O_j^*(it) = -(O_j(p) - O_{\mathrm{mes}})(it) + \sum_{k=1,k(2)=j}^{N\mathrm{coupl}} (Do_k(p) - Do_{\mathrm{mes}k})(it) \\ (R_O)^* U^*(it) = \sum_{k=0}^{N-it} (R_k)^* U^*(it+k) + \sum_{k=0}^{N-it} (Q_k)^* U(it+k) O^*(p)(it+k) \end{cases} \tag{35}$$

The gradients formulas remain unchanged.

This formulation in ΔP can be applied in the classical or multilinear formulation.

III. Numerical Application: ARIANE 511 Flight Inverse Source Problem

The methodology has been validated on the 511 ARIANE V flight. Thirteen measurements have been acquired. The boundary element method ARIANE V mesh has been realized by the software SDRC IDEAS and is approximately composed of 1000 triangular surface elements. The inverse acoustic analysis has to cover the low-frequency range 4/40 Hz (measurement data are filtered consequently). The size of a typical element is at least 1/5 of the minimal acoustic wavelength of the time domain pulse.

From the measurements data acquired during the 511 flight, one set of sources is searched, corresponding to Fig. 5. The purpose is to define the following:

1) A finite number, as small as possible, of overpressure source locations,

2) Sources as simple as possible. For having easy dynamic response calculations, we have investigated the feasibility to restore the pressure levels measured on the launcher, with sufficient accuracy (within 20%), from isotropic sources. Given our past experience and experience acquired during the space shuttle program [19], we had an idea of the overpressure source locations. Keeping in mind that the overpressure is composed of two pressure waves, the IOP and the DOP, the overpressure sources are located on the launch table (a source per solid rocket booster) and at the launch duct exit (a source per solid rocket booster). The above mentioned source locations are shown in Fig. 5: the DOP sources are at the launch duct exit and the IOP sources on the launch table. In addition, two symmetrical sources of the IOP sources, and two symmetrical sources of the DOP sources, with respect to the mast are included in the set of sources, to take into account the reflection of the IOP and DOP acoustic sources on the mast, which is not represented by a boundary finite element model in the computations. Furthermore, a source representing the Vulcain engine and its image with respect to the mast have been introduced. Indeed, during the intermediate phase between IOP and DOP waves, as waterfall is used at liftoff to reduce the pressure levels, the Vulcain engine has some contribution to the pressure field.

3) In the definitive, we search an equivalent set of 10 sources.

4) The evolution versus time of the pressure levels of the predefined sources and the pressure levels applied to the launcher structures induced by the localized sources (see also [19,20]).

For this study case, one direct code simulation requires a number N of iterations equal to 400 time steps, with a time step of $\Delta t = 4.1e - 3$ s. On a Unix workstation, two days computation are necessary for the whole inversion process ($L = 300$ optimizer iterations).

The time period of interest is between 7 and 8 s. At the beginning of the inverse process, all the sources were set to be equal to zero for this entire time interval. The computations have been performed in three steps:

1) to only identify the IOP sources during the IOP phase,

2) to only identify the DOP sources during the DOP phase,

3) to identify the Vulcain source during the whole overpressure phase and the IOP sources during the DOP phase.

An example of an identified source is presented in Fig. 6.

After identification of the sources, a direct problem is solved, to compute the pressure levels on the locations, where the 13 sensors are mounted. Those simulated pressure levels are compared with the real values measured by the same sensors. Figures 7 and 8 give an example of pressure measured by the fairing sensor 10, and the difference of pressures measured by diametrically opposite sensors 10 and 12. The agreement is quite good in the time domain.

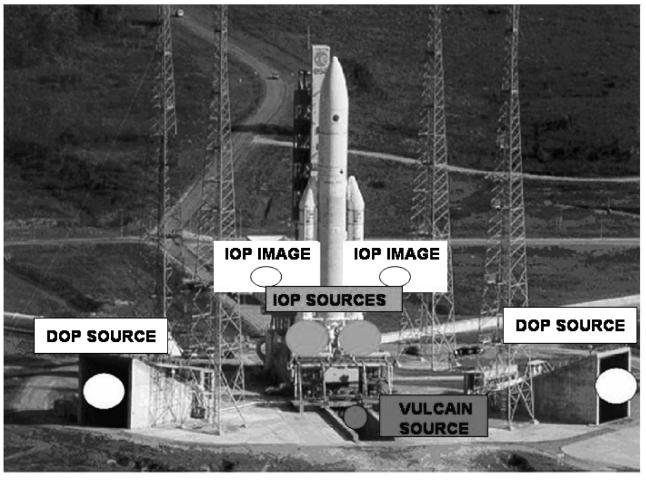

Fig. 5 Locations of overpressure sources.

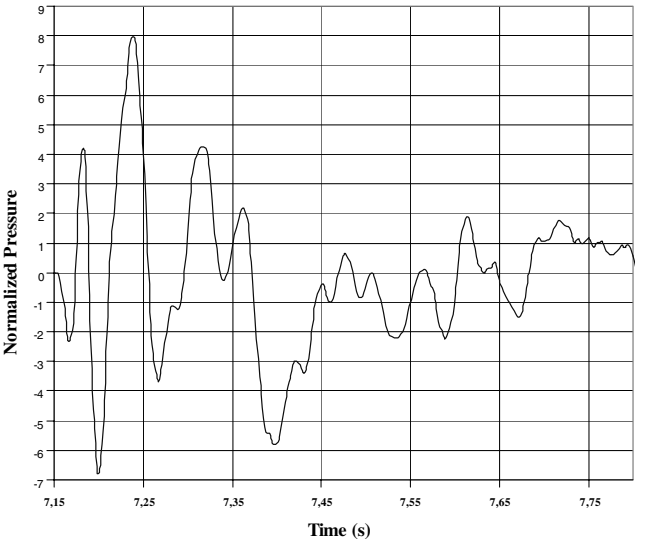

Fig. 6 Evolution of the right SRB source versus time.

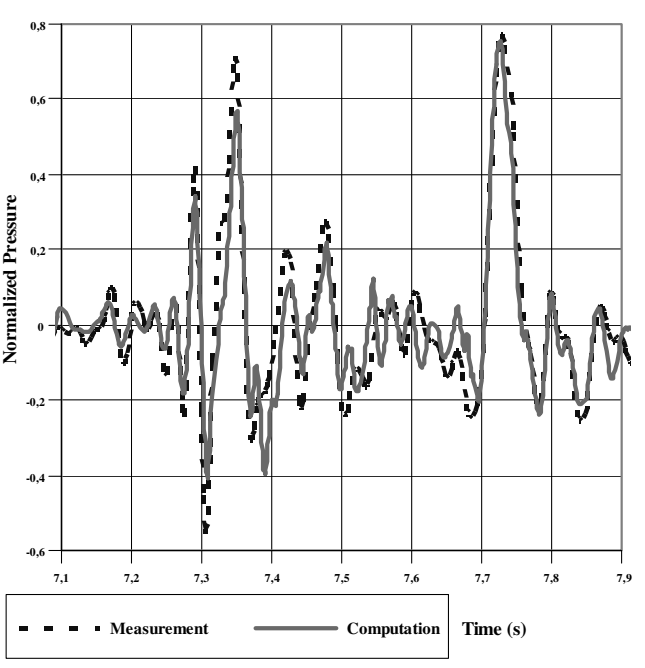

Fig. 7 Comparison of the measured and computed data.

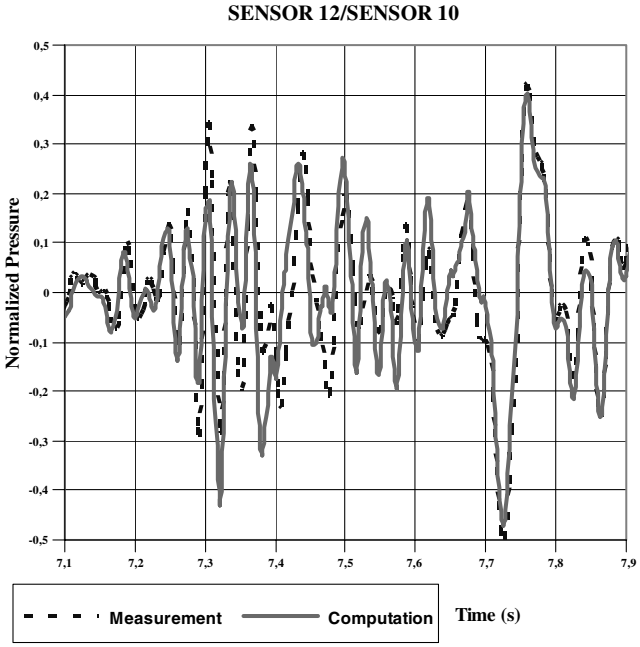

Fig. 8 Comparison of the measured and computed differences of pressure data.

For all sensors, the global error between computed and measured data is no more than 10%, which is very small.

An analysis of the robustness of methodology was achieved. It is related to three aspects:

1) The check that all the restored pressures are physical. Indeed, the inversion and optimization were based on a finite number of measurements mounted on the launcher (four on the upper part and nine on the first stage). It is necessary that the pressures calculated at other points have a physical consistency.

2) The analysis of the impact of the number of measurements mounted on the launcher on the quality of the restitutions. The low number of sensors mounted on the upper part may raise a certain number of questions, with regards to the quality of the restored pressure field on the upper part.

3) The correlation between the identified sources and some propulsion parameters, which were not taken into account in the inverse problem.

Concerning the first point, a direct calculation of pressures at any point of a grid of the launcher ARIANE 5 was carried out. This grid (Fig. 9) consists of approximately 30 sections, each containing eight points of calculation.

The analysis of the computed pressures shows a regular and a continuous distribution of pressures for all the sections (Figs. 10 and 11), and an expected change of the pressures with the distance to the nozzle exit planes, with a fast decrease with the distance near the sources and a slow decrease for the points of the upper part far from the sources.

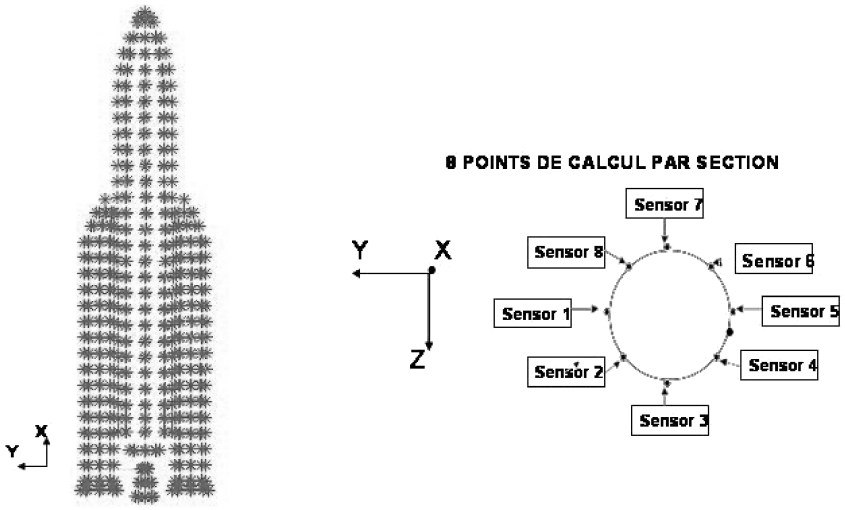

Fig. 9 Grid of the launch vehicle and location of computation points per section.

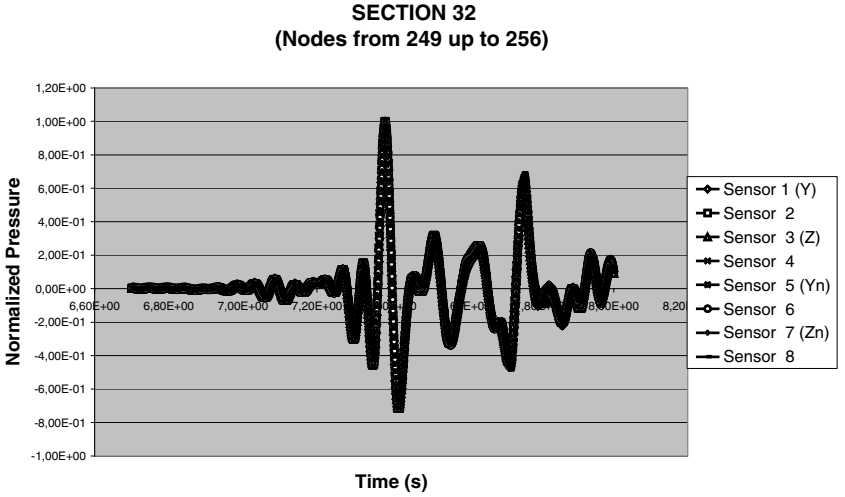

Fig. 10 Analysis of the computed pressure field (repartition per section).

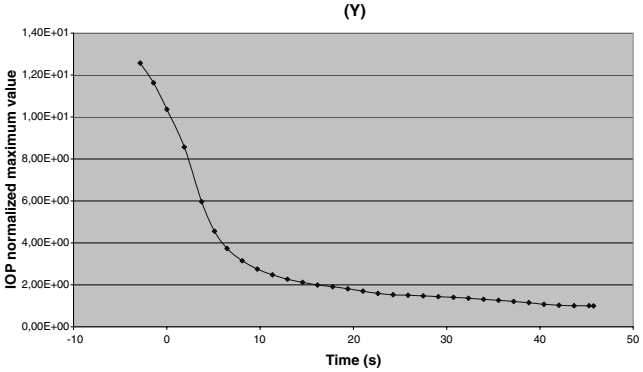

Fig. 11 Analysis of the computed pressure field (IOP normalized maximum value).

Concerning the analysis of the impact of the number of measurements on the quality of the restitutions, a drastic approach has been chosen: identification was achieved by withdrawing the four measurements of the high part and comparing them with measurements of the upper part (Figs. 12 and 13).

The comparison of the calculated and restored pressures shows a light degradation of the restitution (Fig. 12) for the sensor 10. This measurement point has been chosen, because it is on the upper part, part of the launcher on which measurements were not taken into account within the framework of this robustness study on one hand, and, on the other hand, it is important to restore the pressure field of the upper part with a very great accuracy, to determine the dynamic loads applied to the payloads. Nevertheless, the frequencies are always respected. Degradation is stronger on the pressure differences, but the peaks are simulated (Fig. 13). This result can be explained by the great number of measurements on the lower part of the launch vehicle, at distances from 6, 13, and 20 m of the gimbal point Cardan joint of the central engine. These measurements allow one to restore the strong decrease for the points close to the engines and the weak slope for the points far away (Fig. 12) (pressure pattern along the generator Y). Consequently, the number of measurements were sufficient to characterize the pressure field with accuracy.

The third analysis relates to the correlation between the measured sources IOP and propulsion parameters measured in flight. Indeed, it is shown in the literature [3] that the intensity of the overpressure depends on the derivative, with regard to time, of the pressure in the combustion chamber. This pressure is not directly measured.

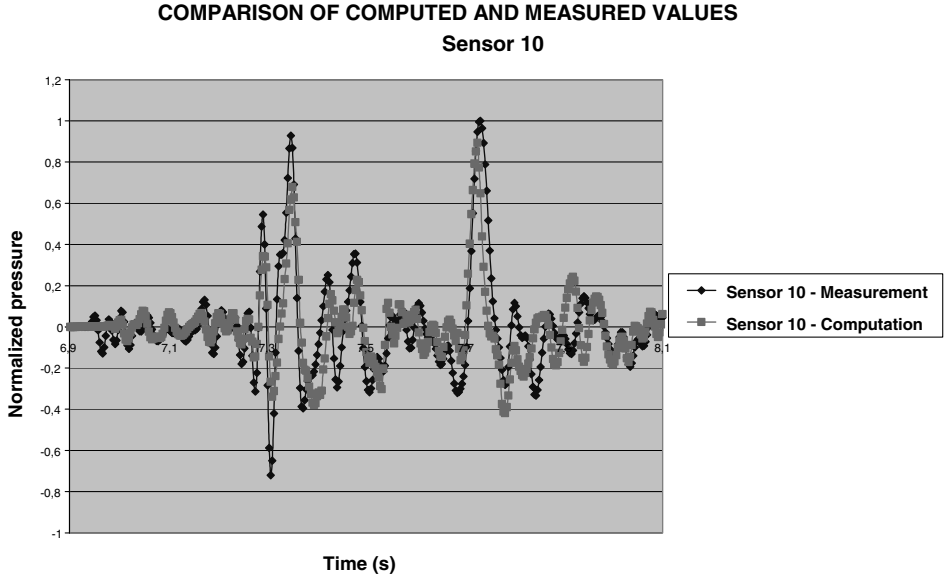

Fig. 12 Analysis of the computed pressure field without taking into account the upper part measurements.

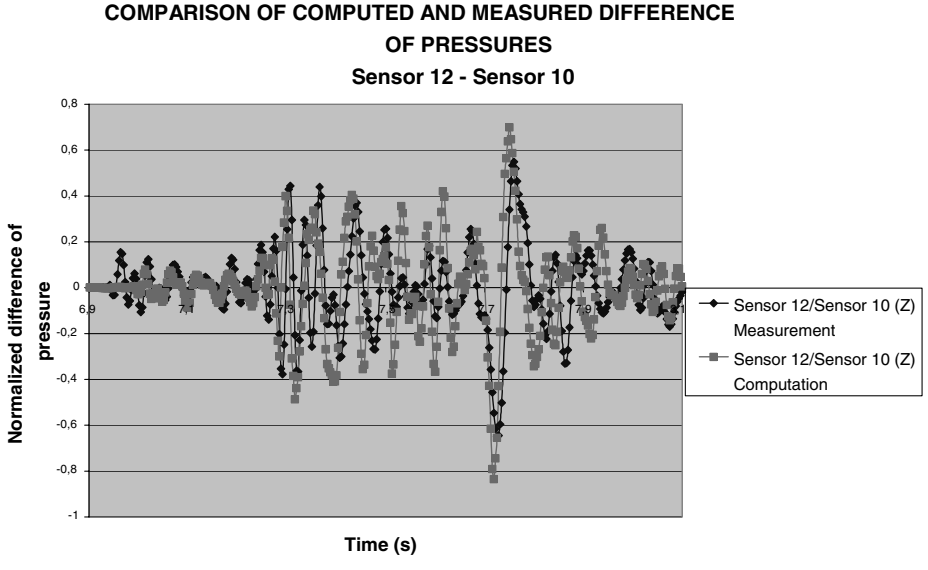

Fig. 13 Analysis of the computed difference of pressure Δp without taking into account the upper part measurements.

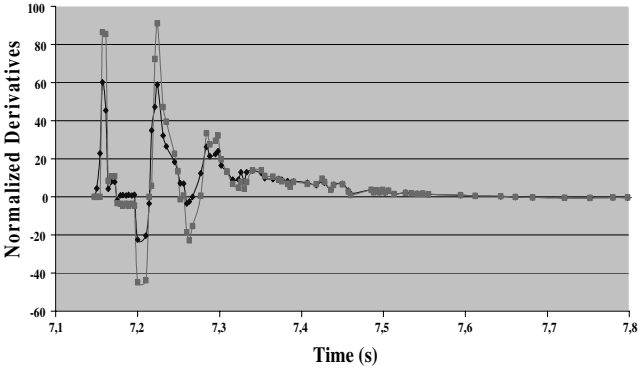

Fig. 14 Derivatives of normalized stagnation and rear static pressure versus time.

However, the stagnation and rear static pressures, to which the pressure in the combustion chamber is related, were measured during flight 511. The derivatives of these pressures were calculated. These derivative present peaks (Fig. 14) to which the intensity of the overpressure is connected. If one compares the temporal changes of propulsion measurements and of the amplitude of the source IOP which was identified (Fig. 6), we also observe peaks in correspondence with the peaks observed at the propulsion measurements. It is noticeable that the evolution of the right SRB source against time presents peaks, which appear at nearly the same time (with a time delay of about 0, 2 s) on the evolution of derivatives, versus time, of the SRB stagnation and rear static measured pressures. It is well known [3] that the overpressure depends strongly on the derivative versus time of the combustion chamber pressure. As the measured propulsion parameters have not been taken into account in the inversion process, this feature points out that the identified sources have a physical meaning. This fact demonstrates that the identified sources are not only virtual, but that they have a physical meaning.

IV. Conclusions

A methodology for characterizing the overpressure appearing at ARIANE 5 liftoff has been developed and validated on the 511 flight, using a robust and accurate time domain integral solver for wave propagation.

The corresponding time marching scheme for the direct acoustic source problem is unconditionally stable [no Courant, Friedrichs, Lewy (CFL) conditions]. This allows a classical optimization approach for the inverse problem.

Direct and adjoint codes have exactly the same properties and have been implemented in power parallel computers. Some new developments of this inverse computation method, including the identification of overpressure sources, which restore the measured pressures and above all, the difference of pressure between diametrically opposite points and the reduction of the computation times by a factor of 10 by decomposing the sources parameters into a base of unitary sources (multilinear process), allow the industrial application of such an inverse problem.

We demonstrate the interest of the method on some examples of source reconstructions in low-frequency acoustics for the ARIANE 5 overpressure source identification on the data from the 511 ARIANE 5 flight, with a prior knowledge of the localization of sources: results show a good identification of the multiparameter sources in the 0–40 Hz frequency domain (source function at each time step), with partial acoustic data (launcher upper part sensors). The work was facilitated by the prior knowledge of the acoustic source location.

Furthermore, a complete robustness analysis has been performed to check that the pressures computed at points different from actual measurements are physical. Future work will include:

1) the improvement of the optimizer,

2) the development of a preprocessing tool to identify the sources in the frequency domain in a rational way without hypothesis of their locations,

3) the investigation of predictive capabilities of the inverse method,

4) the increase of the capability of the inverse method to identify the acoustic sources at higher frequencies,

5) the definition and validation of the methodology for identifying random acoustic sources. The additional difficulty brought on by the identification of the acoustic sources at liftoff is linked to the random nature of the acoustic field of interest. A particular investigation will be led to perform in a correct way the identification of acoustic sources by using the intercorrelation matrix of the measurements. Of course, this methodology has a sense of whether the random pressure field is stationary and ergodic.

Acknowledgements

This work was carried out at the European Aeronautic Defence and Space Company Corporate Research Center (EADS CRC) and was supported by EADS Space Transportation, Les Mureaux, and the CNES (Centre National d'Etudes Spatiales, France).

References

[1] Troclet, B., Chemoul, B., Roux, P., Gely, D., and Elias, G., "Synthesis of Vibroacoustic Studies Performed During ARIANE 5 Program," *Proceedings of the First European Conference on Launcher Technology. Launch Vehicle Vibrations*, CNES, Toulouse, France, 14–17 Dec. 1999, pp. 319–326.

[2] Troclet, B., Depuydt, M., and Rohne, P. B., "Experimental Analysis of Aerodynamic Noise on the Launch Vehicle Upper Part," *16th AIAA Aeroacoustics Conference*, AIAA, Washington, D.C., 12–15 June 1995.

[3] Ikawa, H., and Laspesa, F. S., "Ignition/Duct Overpressure Induced by Space Shuttle Solid Rocket Motor Ignition," *Journal of Spacecraft and Rockets*, Vol. 22, No. 4, 1985, pp. 4841–488.

[4] Alestra, S., Terrasse, I., and Troclet, B., "Inverse Method for Identification of Acoustic Sources at Launch Vehicle Lift-Off," *AIAA Journal*, Vol. 41, No. 10, Oct. 2003, pp. 1980–1987.

[5] Ha Duong, T., "Equations Intégrales pour la Résolution Numérique des Problèmes de Diffraction d'ondes Acoustiques," Ph.D. Thesis in Mathematics, Université Paris VI, Paris, France, Sept. 1987.

[6] Hamdi, M. A., "Une Formulation Variationnelle par les Équations Intégrales pour la Résolution de l'Équation de Helmholtz avec des Conditions aux Limites Mixtes," *Comptes Rendus à l'Académie des Sciences, Série II*, Vol. 292, 1981, pp. 17–20.

[7] Becache, E., and Ha-Duong, T., "A Space-Time Variational Formula for the Boundary Integral Equation in a 2D Elastic Crack Problem," *Journal of Mathematics Modelling and Numerical Analysis*, Vol. 28, No. 2, 1994, pp. 141–176.

[8] Bluck, M. J., and Walker, S. P., "Time-Domain BIE Analysis of Large Three-Dimensional Electromagnetic Scattering Problems," *IEEE Transactions on Antennas and Propagation*, Vol. 45, No. 5, May 1997, pp. 894–901.

[9] Dodson, S. J., Walker, S. P., and Bluck, M. J., "Implicitness and Stability of Time Domain Integral Equation Scattering Analyses," *ACES Journal*, Vol. 13, No. 3, Nov. 1998, pp. 291–301.

[10] Gres, N. T., Ergin, A. A., Shanker, B., and Michielssen, E., "Integral Equation Based Analysis of Transient Electromagnetic Scattering from Three Dimensional Inhomogeneous Dielectric Objects," *Proceedings of the 16th Annual Review of Progress in Applied Computational Electromagnetics*, Naval Postgraduate School, ACES '00, sponsored by Applied Computational Electromagnetics Society, Monterey, CA, 20–24 March 2000, pp. 647–653.

[11] Abboud, T., El Gharib, J., and Zhou, B., "Retarded Potentials for Acoustic Impedance Problems," *Proceedings of the 5th International Conference on Mathematical and Numerical Aspects of Waves Propagatio*, sponsored by INRIA and SIAM, edited by SIAM, INRIA, Saint Jacques de Compostelle, Spain, July 2000, pp. 703–709.

[12] Alestra, S., "Méthodes Inverses en Électromagnétisme pour des Milieux Stratifiés, Bipériodiques et Bidimensionnels," Ph.D. Thesis in Mathematics, Department of Mathematics, Université Paris XIII, Villetaneuse, France, July 1997.

[13] Terrasse, I., "Résolution Mathématique et Numérique des Équations de Maxwell Instationnaires par une Méthode de Potentiels Retardés,"

Ph.D. Thesis in Mathematics, Department of Applied Mathematics, Ecole Polytechnique, Palaiseau, France, Jan. 1993.

[14] Terrasse, I., "Résolution des Équations de Maxwell Instationnaires par une Méthode de Potentiels Retardés," *Proceedings of the European Symposium on Numerical Methods in Electromagnetics JEE'93*, sponsored by ONERA, INRIA, MIP, Toulouse, JEE, 17–19 Nov. 1993, pp. 135–141.

[15] Terrasse, I., Ludwig, B., Alestra, S., Duceau, E., and Ha Duong, T., "Inverse Acoustic Impedance Problem Using the Delayed Time-Domain Boundary Integral Method," *Proceedings of the 5th International Conference on Mathematical and Numerical Aspects of Waves Propagation*, sponsored by INRIA and SIAM, edited by SIAM, INRIA, Saint Jacques de Compostelle, Spain, July 2000, pp. 667–671.

[16] Ludwig, B., "Etude de Quelques Problèmes Directs et Inverses en Propagation d'ondes Acoustiques Transitoires. Méthodes d'Eléments Finis de Frontière," Ph.D. Thesis in Mathematics, Department of Applied Mathematics, Université de Compiègne, Compiègne, France, Nov. 2000.

[17] Bamberger, A., Chavent, G., and Lailly, P., "About the Stability of the Inverse Problem in 1D Wave Equation," *Journal of Applied Mathematics and Optimization*, Vol. 5, 1979, pp. 1–47.

[18] Lions, J. L., *Contrôle Optimal des Systèmes Gouvernés par des Équations aux Dérivées Partielles*, Dunod, Paris, 1968.

[19] Ikawa, H., and Laspesa, F. S., "Space Shuttle SRM Ignition Overpressure Prediction Methodology," *JANNAF 13th Plume Technology Meeting*, CPIA Pub. 357, April 1982, pp. 245–256.

[20] Freund, J. B., Lele, S. K., and Moin, P., "Numerical Simulation of a Mach 1.92 Turbulent Jet and Its Sound Field," *AIAA Journal*, Vol. 38, No. 11, 2000, pp. 2023–2031.

M. Miller
Associate Editor